

Nanoscale

Accepted Manuscript



This is an *Accepted Manuscript*, which has been through the Royal Society of Chemistry peer review process and has been accepted for publication.

Accepted Manuscripts are published online shortly after acceptance, before technical editing, formatting and proof reading. Using this free service, authors can make their results available to the community, in citable form, before we publish the edited article. We will replace this *Accepted Manuscript* with the edited and formatted *Advance Article* as soon as it is available.

You can find more information about *Accepted Manuscripts* in the [Information for Authors](#).

Please note that technical editing may introduce minor changes to the text and/or graphics, which may alter content. The journal's standard [Terms & Conditions](#) and the [Ethical guidelines](#) still apply. In no event shall the Royal Society of Chemistry be held responsible for any errors or omissions in this *Accepted Manuscript* or any consequences arising from the use of any information it contains.

Cite this: DOI: 10.1039/c0xx00000x

www.rsc.org/ xxxxxx

PAPER

Nitrogen-enriched double-shelled carbon/layered double hydroxide hollow microspheres for excellent electrochemical performance

Jie Xu, Fei He,* Shili Gai, Shenguan Zhang, Lei Li and Piaoping Yang*

Received (in XXX, XXX) Xth XXXXXXXXXX 20XX, Accepted Xth XXXXXXXXXX 20XX

DOI: 10.1039/b000000x

A unique double-shelled hollow carbon-based composite with enriched nitrogen has been prepared through a facile and versatile synthetic strategy. The hierarchical composite employs the nitrogen enriched carbon hollow sphere as an interior shell and intercrossed Ni/Al layered double hydroxide (LDH) nanosheets as an exterior shell. The as-obtained N-C@LDH hollow microspheres (HMS) have high nitrogen enrichment, large specific surface area (337 m²/g), uniform and open mesoporous structure. Taking advantage of these characteristics, the composite exhibits obviously superior capacitive behavior to that of nitrogen-free carbon@LDH composite and hollow LDH without carbon shell, including high specific capacitance, excellent rate capability, and good cycling stability. The composite displays high specific capacitance of 1711.51 F/g at a current density of 1 A/g. In particular, the high specific capacitance can be kept to 997.3 F/g at a high current density of 10 A/g, which still retains 94.97% after 500 cycles at this high current density. This N-enriched hollow carbon/LDH composite can be expected to be a promising electrode material for electrochemical capacitors due to its high electrochemical performance.

1. Introduction

With the decreasing availability of fossil fuels and increasing demand of clean energy, supercapacitors, as emerging energy storage devices, have attracted intensive interest owing to high power density, long cycle life, short charging time and good safety record. In general, supercapacitors can be divided into two types in terms of different operating mechanisms of energy storage process.¹⁻³ The first one is electric double-layer supercapacitors (EDLCs) storing energy by ion adsorption, and taking carbon-based materials as active materials. The other one is pseudo-capacitors storing energy through fast surface redox reactions and commonly using transition metal oxides and hydroxides as electrode materials. Despite the great advance achieved in the field of supercapacitors,⁴⁻⁹ the electrode materials are still seriously hindered in their practical applications owing to the relatively poor performance, such as low specific capacitance in carbon-based materials, poor cycling stability in transition metal oxides, and very high cost of RuO₂ based materials.¹⁰⁻¹³ Therefore, it is highly promising to design a composite containing both carbon and transition metal oxide as the supercapacitor electrode material, which can combine the advantages and mitigate the shortcomings of both components. In other words, it would be interesting to effectively combine the EDLCs and pseudo-capacitor by developing a hybrid type of electrode materials, where electric double-layers and faradaic capacitance can be realized concurrently to contribute to the high energy density and better overall performance.^{12,14,15}

Carbon materials have been regarded as the most popular electrode materials owing to their superior physical and chemical properties, including low cost, light weight, large surface area, diverse forms (powders, monoliths, fibers, sheets, aerogels, and tubes), good processability, adjustable porosity, relatively inert electrochemistry and electrical conductivity.^{7,12,16} However, with the rapid depletion of fossil fuels and environmental pollution issues, the simple carbon materials cannot meet the increasing demands in the field of electrical energy storage and conversion. Hence, to further expand the properties of carbon materials, surface and/or framework modification has been widely investigated because the properties of carbon materials are closely related with the raw material, surface structure and porosity. Moreover, heteroatoms dopant can modify the electron/donor characteristics and crystalline structures of the carbon host, and further exert large effects on physicochemical properties of carbon-based materials.¹⁷⁻¹⁹

Recently, boron,^{6,20} nitrogen,^{21,22} boron-nitrogen,^{23,24} phosphorus²⁵ nitrogen-phosphorus,²⁶ and sulfur²⁷ have been extensively employed as dopants to improve the electrochemical performance of carbon-based materials. Among those, nitrogen dopant is attractive due to its higher electro-negativity for its smaller atomic diameter.²⁸ The N-doping in the carbon host can increase surface polarity, enhance electric conductivity, improve the wettability of carbon matrix with electrolyte, and introduce active basic/catalytic sites to the carbon surface.^{8,17} Such nitrogen-containing carbon materials with enhanced performance are of significant importance to the frontiers of many domains,

such as electrical capacitors,^{18,29-31} lithium batteries,^{23,28} fuel cells,^{32,33} catalysis,³⁴⁻³⁷ sensing,²² biological field,³⁸ and adsorption and separation.^{17,39,40} There are two general processes for incorporating nitrogen into hosts. One is post-treatment of carbon materials with ammonia amines, urea or pyridine to introduce nitrogen-containing groups on the surfaces.^{21,41-44} The other is *in situ* homogeneously doping using nitrogen containing precursors, including melamine resorcinol-formaldehyde (RF),^{17,38,45} polypyrrole,⁴⁶ acetonitrile,⁴⁷ acrylonitrile,⁴⁸ polyaniline,^{29,49} terephthalonitrile,³⁶ and biomass derivatives.^{50,51}

As stated above, the N-doped carbon materials have attracted intensive interest in the application of electrode materials. Besides, layered double hydroxides (LDHs) containing transition metal elements, have been reported to be a kind of interesting electrode materials for supercapacitors, which is due to their relatively low cost, environmentally friendly nature and high redox activity.^{13,52-56} The key challenge for the application of LDHs in supercapacitors is to fabricate a well-defined architecture with large surface area and mesoporous pore size distribution, which are benefit for the mass and electron transfer of electrochemical process. It is well known that the aggregation of active materials tends to reduce the accessible surface area for participating electrochemical reaction, which in turn decreases the specific capacitance. And the low conductivity of pseudocapacitive materials can also restrict the electron-transfer rate, resulting in inferior performance at high charge-discharge current density.^{13,54} Thus, it is expected to be an excellent supercapacitor material consisting of LDHs with large specific surface and N-doped carbon material with good conductivity.

Herein, we designed a double-shelled hollow carbon-based composite combining nitrogen-doped carbon hollow microspheres and NiAl-LDH nanosheets. This interesting structure uses the nitrogen-enriched porous carbon hollow sphere as an interior shell, and adopts the curly NiAl-LDH nanosheets straightly grown on the carbon sphere in formation of an urchin-like exterior shell. The composite possesses the unique architecture and homogenous element distribution as desired. In particular, the composite exhibits high electrochemical performance due to the N doping deduced enhanced conductivity, larger specific area and favorable porous structure. Due to the high specific capacitance, outstanding rate capability, and excellent cycling stability, the composite should be a promising electrode material for supercapacitors.

2. Experimental section

2.1. Synthesis

Silica microspheres. The monodisperse silica microspheres with particle size of 450 ± 20 nm were obtained by hydrolysis of tetraethyl orthosilicate (TEOS) in an alcohol medium containing water and ammonia *via* a modified Stöber process.^{57,58} Typically, the solution containing TEOS, H₂O, ammonia (NH₄OH) and ethanol with the concentration ratio of 0.7: 1.4: 8.2: 5.3 was stirred at room temperature for 6 h, leading to the white silica colloidal suspension. The obtained product was separated by centrifugation and washed with H₂O and ethanol for several times.

Carbon HMS and N-enriched carbon HMS. The core-shell

SiO₂@RF was prepared by a polymer coating process.⁵⁹ 0.5 g of as-obtained SiO₂ spheres was dispersed in 44 mL of H₂O by ultrasonication. 1.4 g cetyltrimethylammonium bromide (CTAB), 0.22 g resorcinol, 17.6 mL ethanol and 0.1 mL NH₄OH were added in the SiO₂ suspension continuously. By stirring 30 min at 35 °C to form a uniform dispersion, 0.3 mL of formalin solution was added to the dispersion under stirring. After another stirring at 35 °C for 6 h, the mixture was naturally cooled to room temperature and then keeping at room temperature overnight. After collecting by centrifugation, the obtained SiO₂@RF was washed with ethanol and water several times and dried at 60 °C for 12 h. With a heating rate of 5 °C/min, the SiO₂@RF was heated from room temperature to 150 °C and kept at this temperature for 1 h under Ar atmosphere. Under the same heating rate and atmosphere, the temperature was then raised to 600 °C and held at this temperature for 3 h. Finally the carbon hollow microspheres (HMS) can be produced by treating the pyrolyzed SiO₂@C with 2 M NaOH at 85 °C for 12 h.

The nitrogen-enriched carbon hollow microspheres were obtained by a post-synthetic process.^{17,39} Typically, 0.1 g of as-prepared SiO₂@RF spheres were mixed with 0.15 g melamine and dispersed in 10 mL methanol. Then the suspension was stirred at room temperature until methanol was fully evaporated. The melamine loaded SiO₂@RF was then heated to 600 °C with a heating rate of 5 °C/min at Ar atmosphere and kept for 2 h. After cooling to room temperature, the product was dried at 60 °C. Mesoporous nitrogen contained carbon HMS were obtained after moving SiO₂ template and denoted as N-C HMS.

N-enriched C@NiAl-LDH, NiAl-LDH and C@NiAl-LDH HMS. Aiming to obtain the N-enriched C@NiAl-LDH HMS, an *in situ* crystallization of the NiAl-LDH shell on the surface of N-C@AlOOH spheres was carried out by the urea hydrolysis method.^{53,54,60} Typically, the AlOOH primer sol was obtained through the hydrolysis process of aluminum isopropoxide.⁶¹ Then the AlOOH coated N-C HMS were prepared by a layer by layer (LBL) method. In detail, 0.3 g N-C HMS were put in the AlOOH sol for stirring at room temperature for 2 h, then the separated samples were washed with ethanol for one time and dried at room temperature. The described process was repeated for ten times to obtain the N-C@AlOOH. Consequently, 0.1 of as-obtained AlOOH coated N-C HMS were immersed into 70 ml solution containing 10 mmol Ni(NO₃)₂ and 0.3 g urea. After stirring for 30 min, the mixture solution was placed in an autoclave at 100 °C for 48 h. The targeted product was separated by centrifugation, washed with ethanol and H₂O for several times and dried at 60 °C for 12 h. The final product was designated as N-C@LDH HMS.

The C@NiAl-LDH HMS and NiAl-LDH HMS were prepared in the similar process, in which C hollow spheres and silica were taken as the support for growing NiAl-LDH nanosheets. To discuss the role of AlOOH played in structure of the final composite, a comparison experiment was conducted according to the similar process without the AlOOH coating process.

2.2. Characterization

Powder X-ray diffraction (XRD) patterns were recorded on a Rigaku D/max TTR-III diffractometer equipped with Cu K α radiation ($\lambda = 0.15406$ nm). Fourier-Transform IR (FT-IR) spectra of as-prepared products were carried on a Perkin-Elmer

580B IR spectrophotometer using the KBr pellet technique. The X-ray photoelectron spectroscopy (XPS) was recorded on a VG ESCALAB MK II electron energy spectrometer. Scanning electron microscopy (SEM, Hitachi S-4800) was taken to measure the morphology of the samples. Energy dispersive X-ray spectrometry analyzer (EDS, INC250, Japan Electronic) equipped with SEM was to assess the elements in the products. Transmission electron microscopy (TEM) and high-resolution transmission electron microscopy (HRTEM) were performed on a FEI Tecnai G² S-Twin transmission electron microscope with a field emission gun operating at 200 kV. N₂ adsorption/desorption isotherms were measured at -196 °C by using a Micromeritics TriStar 3020 instrument. The specific surface areas were determined by the Brunauer-Emmett-Teller (BET) method and the pore size distributions were calculated using Barret-Joyner-Halenda (BJH) method.

2.3. Electrochemical measurements

The electrochemical performance of as-prepared products as working electrode materials were investigated using CHI660D electrochemical workstation in 6 M KOH aqueous electrolyte at room temperature. Typically, the working electrode was prepared by coating the viscous slurry of as-obtained active material (80 wt.%; N-C@NiAl-LDH HMS, C@NiAl-LDH HMS and NiAl-LDH HMS), conductive agent (15 wt.%; acetylene black) and binder (5 wt.%; polytetrafluoroethylene, PTFE) in a small amount of absolute alcohol onto the Ni foam. After drying at 60 °C in a vacuum oven for 8 h, the as-formed working electrode, a saturated calomel electrode (SCE, the reference electrode), and Pt foil (1 cm × 1 cm, the counter electrode) form a conventional three-electrode cell for the electrochemical measurements, including cyclic voltammograms, galvanostatic charge/discharge curves, and electrochemical impedance spectroscopy (EIS).

3. Result and discussion

3.1. Formation, phase, morphology properties.

The synthetic protocol of all the active materials is showed in the Scheme 1. The SiO₂ spheres obtained from a stöber process were employed as hard templates. A uniform RF layer is



Scheme 1 Schematic illustration for the formation process of N-C@LDH HMS, C@LDH HMS and LDH HMS.

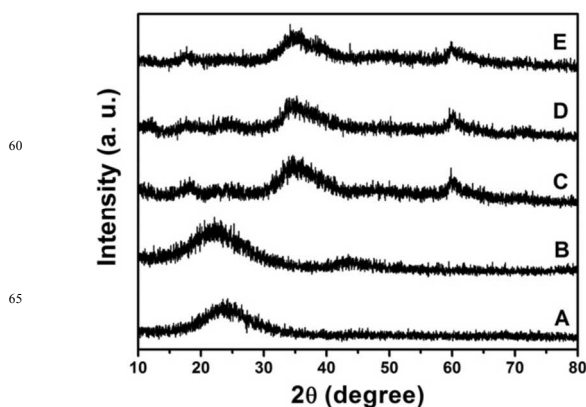


Fig. 1 XRD patterns of as-prepared carbon HMS (A), N-doped carbon HMS (B), NiAl-LDH HMS (C), C@NiAl-LDH HMS (D) and N-C@NiAl-LDH HMS (E).

self-assembly on the SiO₂ core with the assistance of cationic surfactant CTAB, which was taken as a soft template for *in situ* polymerized RF. Then the as-prepared SiO₂@RF spheres were transformed into SiO₂@C upon the heat treatment under Ar atmosphere at 600 °C for 3 h. The N-doped SiO₂@C was obtained in the similar process just undergoing a simple post-synthetic route with melamine. Then the SiO₂ cores were removed to form carbon HMS and N-doped carbon HMS in 2 mol/L NaOH solution at 85 °C. Finally, the SiO₂, carbon HMS and N-doped carbon HMS were applied as the substrates for the deposition of AlOOH sol and the further *in situ* growth of NiAl-LDH shell.

Fig. 1 shows the XRD patterns of as-obtained carbon HMS, N-C carbon HMS, LDH HMS, C@LDH HMS and N-C@LDH HMS, respectively. It can be seen that the carbon HMS without (Fig. 1A) and with (Fig. 1B) N-doping show similar diffraction features. The patterns show two broad peak at 22–25° and 43.7°, which can be assigned to the (002) and (100) plans of graphite, respectively.^{6,26} The peak shifts to a smaller angle after the nitrogen doping process (Fig. 1B), corresponding to an increased inter-graphite layer distance, which may be due to the increased defects derived from the developed porous structure.⁸ Moreover, the appearance of peak at 43.7° in the N-C hollow spheres indicates that the order of amorphous structure has improved towards a turbostratic type of carbon, which may be due to the addition pyrolysis process in the N-doped procedure.^{51,62} The pattern (Fig. 1C) of NiAl-LDH HMS show a series of reflections at 11.3°, 24.1°, 34.8°, 39.2°, 59.8° and 60.9°, which correspond to the (003), (006), (012), (015), (110) and (113) reflections of a randomly stacked CO₃²⁻-LDH phase, respectively.^{13,54} It can be observed that (00*l*) reflections with lower intensity indicate a preferential orientation of LDH crystallites with their *ab* plane perpendicular to the carbon HMS.¹³ The XRD patterns of LDH grown on the carbon HMS (Fig. 1D) and N-C HMS (Fig. 1E) have the similar characteristics to that of NiAl-LDH HMS (Fig. 1C), indicating their homologous composition and structure. Moreover, the IR spectrum of N-C@LDH HMS (Fig. S1) can further confirm the existence of CO₃²⁻-LDH phase from the characteristic vibrations of CO₃²⁻.^{52,53}

TEM images of SiO₂, SiO₂@RF, SiO₂@C and carbon HMS are given in Fig. 2. The SiO₂ core (Fig. 2A) consists of uniform

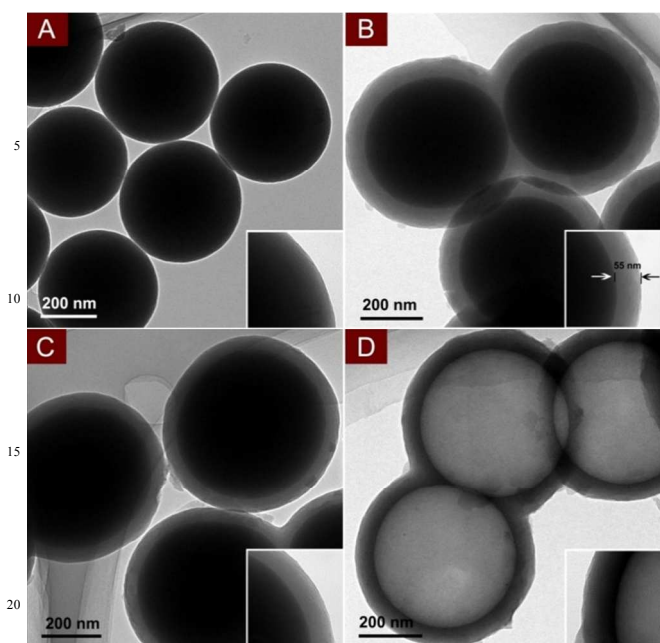


Fig. 2 TEM images of products obtained during the fabrication process: (A) SiO₂ spheres, (B) SiO₂@RF core-shell spheres, (C) SiO₂@C spheres and (D) hollow carbon spheres. Insets are the corresponding magnified TEM images.

microspheres with a diameter of 450 ± 20 nm, smooth surface, and good monodispersity. After the *in situ* polymerization and condensation of resorcinol and formaldehyde, the as-obtained SiO₂@RF (Fig. 2B) has an inorganic-organic core-shell structure with smooth surface and a homogeneous polymer shell thickness (ca. 55 nm). After the carbonization of RF, the as-prepared SiO₂@C spheres (Fig. 2C) well keep the uniform core-shell structure with a shell thickness of about 52 nm, indicating their good mechanical strength. Besides, the slight decrease of shell thickness should be due to the shrinkage of RF during the carbonization process. The carbon HMS (Fig. 2D), converted by the treatment of SiO₂@C with NaOH, well retain the spherical shape with a uniform size of 52 nm and a large void of 450 nm, which is in accordance with the size of SiO₂ core. Close observation (Fig. S2) reveals a large number of tiny micropores on the carbon shell, which may result from the shrinkage of RF and elimination of surfactant (CTAB).⁵⁹

Along with above analysis of carbon hollow spheres, the N-enriched carbon hollow spheres obtained in the similar protocol are described in Fig. 3A and Fig. S3. The SEM image (Fig. 3A) of N-C HMS indicates that the sample retains the spherical shape and hollow interior structure after corrosion by the NaOH solution. The TEM images (Fig. S3 and Fig. 2D) of N-doped and undoped C HMS suggest that they have the similar hollow structure and porous carbon shell. The subsequent LBL process coats a thin AIOOH shell on the as-prepared N-C HMS (Fig. 3B and C). The N-C@AIOOH HMS was transformed into N-C@NiAl-LDH HMS by self-assembly of NiAl-LDH shell on the surface under a hydrothermal treatment. The SEM and TEM images of as-obtained N-C@LDH are depicted in Fig. 3D-H. The SEM image (Fig. 3D) shows that the LDH nanosheets grow uniformly on the carbon wall, constructing a flower-like spherical morphology. The TEM image (Fig. 3E) clearly shows that the 3D

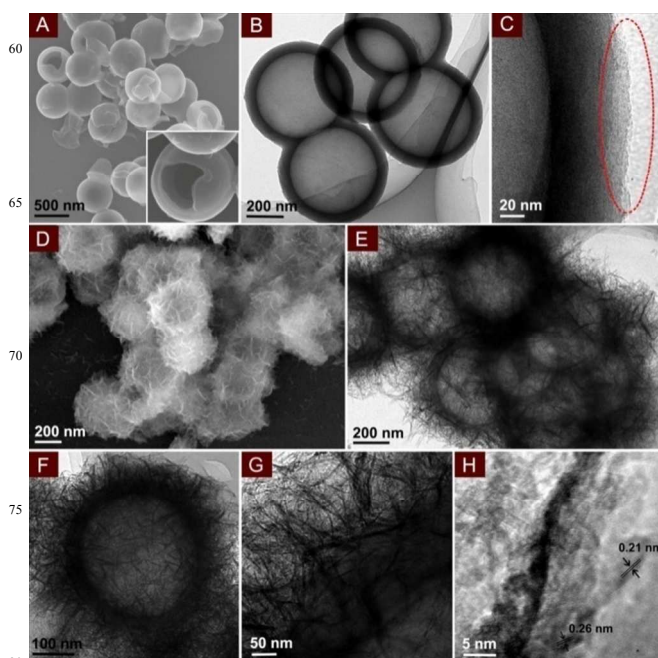


Fig. 3 SEM image of N-C HMS (A), TEM images of N-C@AIOOH HMS (B-C); SEM image (D), TEM images (E-G), and HRTEM image (H) of N-C@LDH HMS. Inset in panel A shows the open pores in a single microsphere.

composite is composed of hollow N-C substance and LDH shell. As displayed, those LDH nanosheets are intercrossed with each other and seem like flexible nanorolls. In a typical TEM image of an individual double-shell hollow structure (Fig. 3F), the thin LDH nanosheets densely cover the surface of N-C HMS and are upon repeated bending and intertangling (Fig. 3G), revealing the good flexibility and high mechanical robustness of NiAl-LDH nanosheets. The HRTEM image (Fig. 3H) displays the distance of 0.21 nm between the adjacent lattice fringes matches well with the d_{015} interplanar spacing of LDH, while the distance of 0.26 nm corresponds to the d_{012} spacing. The SEM images of LDH HMS and C@LDH HMS prepared in the similar process are presented in Fig. S4. It is obvious that they also possess the spherical morphology with hollow structure and urchin-like exterior shell. Notably, SEM image (Fig. S6) of sample prepared without the AIOOH assistance shows that Ni(OH)₂ sheets cannot grow on the surface of N-enriched carbon hollow spheres, indicating that AIOOH sol plays an important role in the formation of double-shelled hollow composite.

Detailed composition and structure information of N-C@LDH HMS are further examined by scanning transmission electron microscopy (STEM) and element mapping analysis. The STEM image (Fig. 4A) of two N-C@LDH HMS spheres also reveals the interesting hollow 3D architecture. The EDS spectrum shows the nitrogen content in the N-C HMS is around 37.6 at.% (Fig. S5). Through the *in situ* growth process, the nitrogen loading content in the composite still achieves 10.53 at.% (Fig. 4B). Ni, Al elements are found and no Si element can be detected, confirming the existence of LDH in the composite and the complete removal of SiO₂. The STEM-EDX line analysis of the microspheres along the noted path (Fig. 4C) is shown in Fig. 4C. As described, the appeared C, N and Ni curves further reveal the hollow structure.

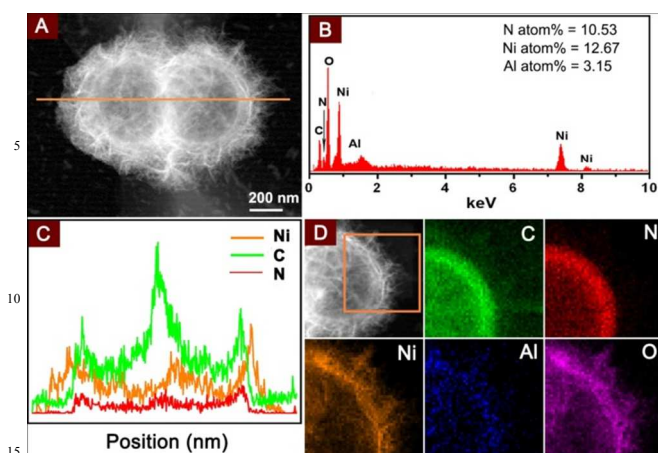


Fig. 4 STEM image (A), EDS analysis (B), STEM-EDX line analysis (C) of the two hollow microspheres of N-C@LDH, and the elemental maps (D) of corresponding C, N, O, Ni, and Al in the N-C@LDH HMS.

The different peak positions between the Ni and N elements indicate that N element distributes in the carbon hollow spheres and Ni element appears in the LDHs shell. As expected, EDS mapping analysis of the demisemi-sphere noted in Fig. 4D clearly confirms that the hierarchical structure is constructed by an interior shell of N-C hollow spheres and an exterior shell of urchin-like LDH nanosheets. Besides, it is found that O element appears in both carbon hollow spheres and LDH shell. The high N content in the as-obtained composite suggests that melamine post-treatment process is a feasible route to prepare nitrogen-enriched materials.

The XPS spectra of as-prepared three samples have been given in Fig. S7. The survey XPS spectrum of LDH HMS (Fig. S7A) indicates the presence of C, O, Ni and Al elements in the hollow spheres. In the C 1s spectrum, the peak at 288.5 eV assigned to carboxylate carbon (O-C=O) should come from carbonate of the interlayer in LDHs, which is in accordance to the XRD (Fig. 1) and FT-IR results (Fig. S1). In the Ni 2p spectrum Furthermore, the two major peaks at around 855.9 and 873.5 eV with a spin-energy separation of 17.6 eV are ascribed to the Ni²⁺ in the NiAl-LDH.⁶³ In the case of C@LDH HMS (Fig. S7B), C, O, Ni, and Al elements can be detected. In the C 1s spectrum, the intensity of the C-O peak at 286.5 eV (blue curve) is much stronger than that of NiAl-LDH hollow spheres, which can be due to the successful introduction of carbon shell in the composite. Another peak at around 287.8 eV ascribed to double-bonded carbon (C=O) appears in the C@LDH HMS, which may be owing to the possible existing oxygen-containing functional groups on the carbon surface in carbon-based composite. For N-C@LDH HMS (Fig. S7C), the C 1s spectrum is deconvoluted into four broad peaks around at 284.6, 286.0, 287.5 and 289.0 eV, respectively. Therein, the strongest signals at 284.6 eV derives from the carbon-carbon bonding in a pure carbon environment. And the peak at 286.0 eV can be ascribed to several possible structures including C-N and C-O functionalities. The peaks centered at 287.5 and 289.0 eV can be mainly associated with the carbon atoms in quinine and/or pyridine and carboxyl groups, respectively.^{17,29} In the N 1s spectrum, the spectrum can be fitted by four peaks centered at about 398, 400, 401, and 403 eV, which are assigned to pyridinic (N-6), pyrrolic/pyridine

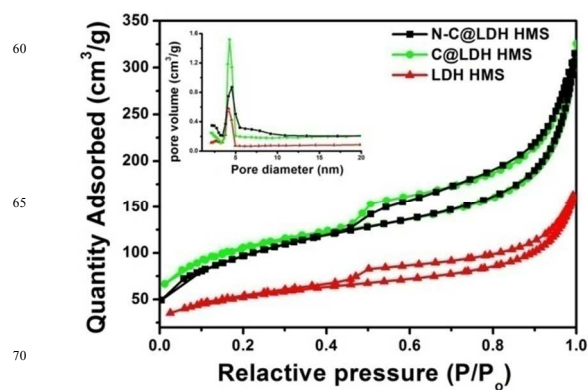


Fig. 5 N₂ adsorption/desorption isotherms and pore size distribution (inset) of as-obtained LDH HMS, C@LDH HMS, and N-C@LDH HMS.

(N-5), quaternary (N-Q) nitrogen, and pyridine N-oxide (N-X), respectively.^{18,64} As reported previously, the presence of N-5 and N-6 can lead to great pseudocapacitance effect and thus increases the capacitance performance.^{29,65}

The nitrogen adsorption/desorption isotherms of the three hollow electrode materials and derived pore size distributions are plotted in Fig. 5. It shows that all the isotherms are type IV with distinct hysteresis loops, indicating all the samples own mesoporous feature.^{7,54} The results can be further conformed by the pore size distribution analysis by the BJH method (inset in Fig. 5). The BET specific surface areas of the obtained NiAl-LDH HMS, C@NiAl-LDH HMS and N-C@NiAl-LDH HMS are 183, 356, and 337 m²/g, respectively. The corresponding pore volume and the pore size are 0.24 cm³/g and 6.67 nm; 0.41 cm³/g and 7.05 nm; 0.35 cm³/g and 6.83 nm, respectively. As expected, the carbon composites possess a larger specific surface area and pore volume than those of pure LDH HMS. Moreover, the N-enriched carbon composite obtained by a post-process has a slightly decreased BET specific surface area and pore volume, which is reasonable since a further heat treating is favourable for the high crystallinity of carbon interior shell.^{7,17}

3.2. Electrochemical performance of N-C@LDH HMS.

Based on the characterization results of N-C@LDH HMS, there are abundant micropores and mesopores inside the 3D structured composite, which would benefit specific surface area and electrical conductivity. Furthermore, the urchin-like LDH nanosheets on the surface of N-C HMS would give rise to pseudo-capacitance. As a consequence, the as-obtain N-enriched double-shelled hollow composite is desirable to have a favorable electrochemical performance as electrode materials. The supercapacitor performance of N-C@LDH HMS is evaluated by cyclic voltammetry (CV) and galvanostatic charge-discharge measurement taking 6 mol/L KOH as the aqueous electrolyte. For comparison, the electrochemical performance of C@LDH HMS and LDH HMS was studied under the same condition.

CV curves of LDH HMS, C@LDH HMS and N-C@LDH HMS recorded at a scan rate of 2 mV/s are shown in Fig. 6A. It is obvious that all the CV curves of three products have a couple of redox peaks, indicating the existence of the Faradaic process. As described in the equation (1), the redox peaks can be ascribed to the faradaic redox reactions related to Ni-O/Ni-O-OH.^{56,66}

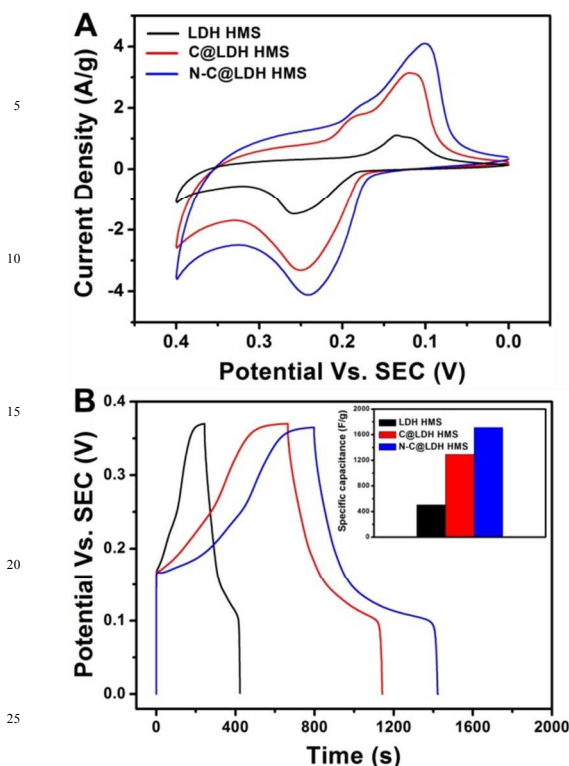


Fig. 6 Electrochemical performance of obtained N-C@LDH HMS, C@LDH HMS and LDH HMS as supercapacitor electrodes: CV curve of (A) at a scan rate of 2 mV/s within the operation voltage of 0-0.37 V in the three electrode system; galvanostatic charge-discharge curves and the according specific capacitance (inset) at a current density of 1 A/g for the three electrode materials.



The CV curves demonstrate that the capacitance of the active materials is mainly derived from the pseudocapacitance with its root in the redox pairs of $\text{Ni}^{2+}/\text{Ni}^{3+}$, rather than purely the electric double-layer charging/discharging of hollow carbon spheres at the electrode/electrolyte interface. Moreover, the similar electrochemical behavior of the three electrode materials further demonstrates the existence of LDH in all the products. Compared with pure LDH HMS, the cathodic peaks and anodic peaks of the two carbon-base composites have a little shift, which is owing to polarization effect of the electrodes. Compared to the flower-like LDH HMS, the porous carbon HMS (or N-enriched carbon HMS) with the flower-like LDH shell possesses larger specific surface area and more lateral pathway for electron transport, which derive from interior carbon shell with a large amount of porous structure. Distinctly, the enclosed areas of the C@LDH HMS and N-C@LDH HMS are much larger than that of LDH HMS, declaring the larger specific capacitance for the carbon based composite. It is noted that the N-enriched double shell carbon composite presents the largest specific capacitance among the three active materials, which is due to unique 3D architecture, favorable porous structure and enhanced electrochemical activity coming from the introduction of nitrogen atoms. Fig. 6B shows the charge-discharge curves of the three active materials at the current density of 1 A/g. The inset of Fig. 6B can clearly describe

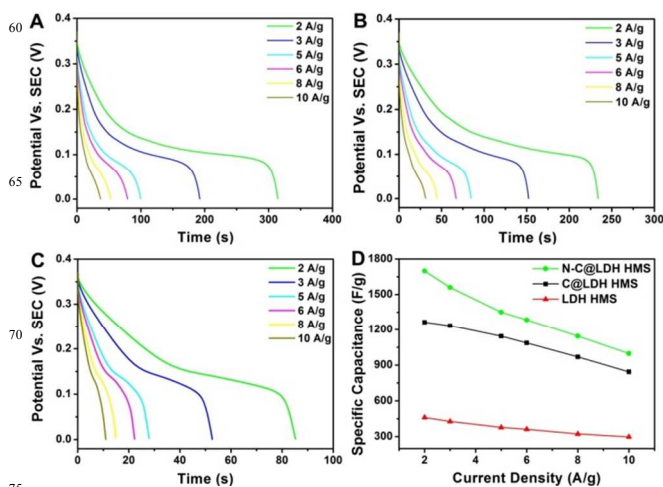


Fig. 7 Discharge curves of N-C@LDH HMS (A), C@LDH HMS (B) and LDH HMS (C) at different current densities, and variation of specific capacitance against different current densities (D).

the specific capacitance of the three electrodes calculated from the equation (2) according to the discharge curves:

$$C = I\Delta t/m\Delta V \quad (2)$$

Where I is the constant discharge current (A), Δt is discharge time (s), ΔV is the potential window (V) and m is the mass (g) of the active material coated on the electrode. The respective specific capacitance of LDH HMS, C@LDH HMS and N-C@LDH HMS is 504.32, 1291.08 and 1711.51 F/g at a current density of 1 A/g, which is in agreement with the analysis of the CV curves in Fig. 6A.

The discharge curves of all the three active materials at different current densities are shown in Figure 7A-C, which all display a typical pseudocapacitive behavior.¹⁴ The discharge curve of N-C@LDH HMS is shown in Fig. 7A. And the corresponding calculated specific capacitance as a function of the discharge current density is 1699.46, 1560, 1350, 1284.32, 1143.78 and 997.3 at the current density of 2, 3, 5, 6, 8 and 10 A/g (Table S1). The capacitance retention is 58.7% with the increase of current density from 2 to 10 A/g. In other words, even at a high current density of 10 A/g, the N-enriched carbon composite still keeps the specific capacitance as high as 997.3 F/g. Thereby, the performance of N-C@LDH HMS is better than that of LDH HMS and C@LDH HMS, as shown in Fig. 7B and Fig. 7C.

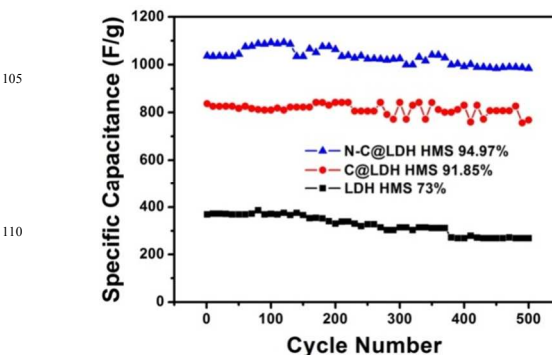


Fig. 8 Cycling performance of the N-C@LDH HMS, C@LDH HMS and LDH HMS (500 cycles).

To assess the electrochemical stability of the N-C@LDH HMS, cycling experiment is carried out with the sample subjected to 500 cycles of charge/discharge at a high current density of 10 A/g in 6 mol/L KOH electrolyte. For comparison, the cycle stability of LDH HMS and C@LDH HMS measured under the same condition is also presented in Fig. 8. For the N-C@LDH, the capacitance is about 94.97% retention (984.9 F/g) after 500 cycles. However the capacitance retention of pure LDH HMS and C@LDH HMS after 500 cycles is 73% (268.92 F/g) and 91.85% (768.38 F/g), respectively. It indicates that the N-enriched composite owns excellent cycle stability with a high specific capacitance compared with that of LDH HMS and C@LDH HMS. It is well acceptable that the introduction of nitrogen atoms in a carbon matrix can improve its electrochemical performance. Firstly, due the higher electronegativity of nitrogen than that of carbon, the involvement of nitrogen atoms can modify the polarity of the carbon matrix, which can improve the wettability of the interface between the electrode and aqueous electrolyte and further enhance the mass-transfer efficiency during the electrochemical process.^{29,67} Secondly, the quantum chemical calculations from Strelko and co-workers show that pyrrol nitrogen, -NH, improves the charge mobility in a carbon matrix by introducing electron-donor characteristics and enhancing the carbon electrochemical activity in electron-transfer reactions, which are caused by a decrease in the ΔE of condensed nitrogen-containing systems.^{65,68} Finally, previous studies showed that the pseudocapacitive interactions take place on negatively charged pyrrolic-N and pyridinic-N, while the positive charge on quaternary-N and pyridinic-N-oxide helped in electron transfer through the carbon.^{18,64,69} In other words, there is very strong dependence of capacitance on the chemistry of surface groups of the carbon. The presence of the quaternary-N within carbon matrix can enhance the conductivity of carbon materials. And the presence of N-5 and N-6 can lead to great pseudocapacitance effect and thus increase the capacitance performance.²⁹ The good stability with high capacitance of N-C@LDH HMS can be attributed to the good mechanical stability and porous structure of carbon shell, and the good conductivity deriving from doped nitrogen atoms. During the cycling process, the increasing trend of capacitance at the initial stage may be owing to the activation process, indicating that unused electrochemically active Ni sites of active material are fully exposed to the electrolyte during the cycling process.^{53,56} However, the slight decrease of capacitance over 500 cycles may be due to a change in the shape, the loss of active surface area and an increase of the resistance during the charge-discharge process.^{53,70}

To understand the reasons for the excellent rate capability of the resulting N-C@LDH HMS, electrochemical impedance spectroscopy is employed to analyze the electrochemical properties of the electrode materials. Fig. 9 shows a Nyquist plot of as-prepared N-C@LDH HMS, C@LDH HMS and LDH HMS in 6 mol/L KOH in a frequency range from 10 kHz to 10 mHz. As displayed, the Nyquist plots for all the three active materials are composed of semicircular shape at high frequencies and linear shape at low frequencies. In general, the size of the semicircle relates to the charge transfer resistance (R_{ct}) at the interface between the electrode material and electrolyte.¹³ From the inset in Fig. 9, it can be seen that the diameter of the semicircle

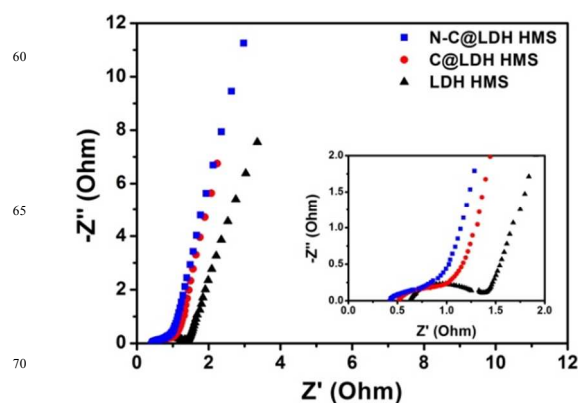


Fig. 9 Nyquist plots of the EIS for as-prepared N-C@LDH HMS, C@LDH HMS and LDH HMS.

decreases in the presence of the porous carbon shell layer, and it further decreases owing to the introduction of nitrogen in the carbon shell, revealing that it enhances the electrical conductivity and improves the interfacial charge transfer in the electrode. Furthermore, the as-designed composite containing N-enriched porous carbon shell can improve the durability and electrochemical properties of the electrode.

4. Conclusions

In summary, a facile and rational process has been designed for the synthesis of nitrogen-doped carbon/NiAl-LDH composite, which contains an interior structure of graphitic porous hollow microspheres by doped nitrogen and an exterior shell constructed by urchin-like LDH nanosheets. The N-doped carbon hollow spheres were successfully obtained with the aid of SiO₂ templates and melamine molecules. The *in situ* growth of NiAl-LDH nanosheets on the surface of carbon wall was realized by a simple hydrothermal treatment with the assistance of AlOOH. The N-doped carbon composite combines the electric double-layer capacitance and pseudo-capacitance with the enhanced conductivity by doping nitrogen. Due to the unique structure, good conductivity and large specific surface area, this nitrogen-enriched double-shelled carbon-based hollow composite exhibits a perfect electrochemical performance. In particular, this strategy may pave a way for the fabrication of other double shelled materials.

Acknowledgements

Financial supports from the National Natural Science Foundation of China (NSFC 21271053), Research Fund for the Doctoral Program of Higher Education of China (20112304110021), Natural Science Foundation of Heilongjiang Province (LC2012C10), Program for New Century Excellent Talents in University, Harbin Sci.-Tech. Innovation Foundation (RC2012XK017012), and the Fundamental Research Funds for the Central Universities of China are greatly acknowledged.

Notes and references

Key Laboratory of Superlight Materials and Surface Technology, Ministry of Education, College of Materials Science and Chemical

- Engineering, Harbin Engineering University, Harbin 150001, P. R. China.
E-mail: yangpiaoping@hrbeu.edu.cn; hefefei1@hrbeu.edu.cn
- † Electronic supplementary information (ESI) available: IR spectrum of N-C@LDH hollow microspheres, Enlarge TEM images of SiO₂@C and carbon hollow spheres, TEM image of N-enriched carbon spheres, SEM images of LDH HMS and C@LDH HMS, EDS analysis of N-enriched carbon spheres, SEM image of the product prepared under the same condition of C@LDH HMS just without the AlOOH sol layer deposited on carbon spheres, survey and element XPS spectra of LDH HMS, C@LDH HMS and N-C@LDH HMS, The specific capacitance of as-prepared N-C@LDH HMS, C@LDH HMS and LDH HMS at different discharge current densities. See DOI: 10.1039/b000000x/
- 1 M. Winter and R. J. Brodd, *Chem. Rev.*, 2004, **104**, 4245.
 - 2 C. Liu, F. Li, L.-P. Ma and H.-M. Cheng, *Adv. Mater.*, 2010, **22**, E28.
 - 3 W. Shi, J. Zhu, D. H. Sim, Y. Y. Tay, Z. Lu, X. Zhang, Y. Sharma, M. Srinivasan, H. Zhang, H. H. Hng and Q. Yan, *J. Mater. Chem.*, 2011, **21**, 3422.
 - 4 Y. Gu, Z. Lu, Z. Chang, J. Liu, X. Lei, Y. Li and X. Sun, *J. Mater. Chem. A*, 2013, **1**, 10655.
 - 5 X. Y. Liu, Y. Q. Zhang, X. H. Xia, S. J. Shi, Y. Lu, X. L. Wang, C. D. Gu and J. P. Tu, *J. Power Source*, 2013, **239**, 157.
 - 6 D.-W. Wang, F. Li, Z.-G. Chen, G. Q. Lu and H.-M. Cheng, *Chem. Mater.*, 2008, **20**, 7195.
 - 7 K. Xie, X. Qin, X. Wang, Y. Wang, H. Tao, Q. Wu, L. Yang and Z. Hu, *Adv. Mater.*, 2012, **24**, 347.
 - 8 B. Xu, H. Duan, M. Chu, G. Cao and Y. Yang, *J. Mater. Chem. A*, 2013, **1**, 4565.
 - 9 J. Jiang, J. Liu, W. Zhou, J. Zhu, X. Huang, X. Qi, H. Zhang and T. Yu, *Energy Environ. Sci.*, 2011, **4**, 5000.
 - 10 G. Zhang and X. W. Lou, *Sci. Rep.*, 2013, **3**, 1470.
 - 11 H. Wang and H. Dai, *Chem. Soc. Rev.*, 2013, **42**, 3088.
 - 12 L. L. Zhang and X. S. Zhao, *Chem. Soc. Rev.*, 2009, **38**, 2520.
 - 13 J. Han, Y. Dou, J. Zhao, M. Wei, D. G. Evans and X. Duan, *Small*, 2013, **9**, 98.
 - 14 Z.-C. Yang, C.-H. Tang, Y. Zhang, H. Gong, X. Li and J. Wang, *Sci. Rep.*, 2013, **3**.
 - 15 X. Huang, X. Qi, F. Boey and H. Zhang, *Chem. Soc. Rev.*, 2012, **41**, 666.
 - 16 M. Oschatz, S. Thieme, L. Borchardt, M. R. Lohe, T. Biemelt, J. Brueckner, H. Althues and S. Kaskel, *Chem. Commun.*, 2013, **49**, 5832.
 - 17 Z. Wu, P. A. Webley and D. Zhao, *J. Mater. Chem.*, 2012, **22**, 11379.
 - 18 D. Hulicova-Jurcakova, M. Seredych, G. Q. Lu and T. J. Bandosz, *Adv. Funct. Mater.*, 2009, **19**, 438.
 - 19 D. Hulicova, J. Yamashita, Y. Soneda, H. Hatori and M. Kodama, *Chem. Mater.*, 2005, **17**, 1241.
 - 20 J. Han, L. L. Zhang, S. Lee, J. Oh, K.-S. Lee, J. R. Potts, J. Ji, X. Zhao, R. S. Ruoff and S. Park, *ACS Nano*, 2013, **7**, 19.
 - 21 H. M. Jeong, J. W. Lee, W. H. Shin, Y. J. Choi, H. J. Shin, J. K. Kang and J. W. Choi, *Nano Lett.*, 2011, **11**, 2472.
 - 22 Y. Wang, Y. Shao, D. W. Matson, J. Li and Y. Lin, *ACS Nano*, 2010, **4**, 1790.
 - 23 Z.-S. Wu, W. Ren, L. Xu, F. Li and H.-M. Cheng, *ACS Nano*, 2011, **5**, 5463.
 - 24 Z.-S. Wu, A. Winter, L. Chen, Y. Sun, A. Turchanin, X. Feng and K. Müllen, *Adv. Mater.*, 2012, **24**, 5130.
 - 25 D. Hulicova-Jurcakova, A. M. Puziy, O. I. Poddubnaya, F. Suarez-Garcia, J. M. D. Tascon and G. Q. Lu, *J. Am. Chem. Soc.*, 2009, **131**, 5026.
 - 26 C. Wang, Y. Zhou, L. Sun, P. Wan, X. Zhang and J. Qiu, *J. Power Source*, 2013, **239**, 81.
 - 27 W. Zhou, H. Chen, Y. Yu, D. Wang, Z. Cui, F. J. DiSalvo and H. D. Abruña, *ACS Nano*, 2013, **7**, 8801.
 - 28 Y. Mao, H. Duan, B. Xu, L. Zhang, Y. Hu, C. Zhao, Z. Wang, L. Chen and Y. Yang, *Energy Environ. Sci.*, 2012, **5**, 7950.
 - 29 Y. Tan, C. Xu, G. Chen, Z. Liu, M. Ma, Q. Xie, N. Zheng and S. Yao, *ACS Appl. Mater. Interface*, 2013, **5**, 2241.
 - 30 L. Zhao, L.-Z. Fan, M.-Q. Zhou, H. Guan, S. Qiao, M. Antonietti and M.-M. Titirici, *Adv. Mater.*, 2010, **22**, 5202.
 - 31 F. Ma, H. Zhao, L. Sun, Q. Li, L. Huo, T. Xia, S. Gao, G. Pang, Z. Shi and S. Feng, *J. Mater. Chem.*, 2012, **22**, 13464.
 - 32 T. Fujigaya, T. Uchinoumi, K. Kaneko and N. Nakashima, *Chem. Commun.*, 2011, **47**, 6843.
 - 33 L. Qu, Y. Liu, J.-B. Baek and L. Dai, *ACS Nano*, 2010, **4**, 1321.
 - 34 H. Wang, T. Maiyalagan and X. Wang, *ACS Catal.*, 2012, **2**, 781.
 - 35 F. Sun, J. Liu, H. Chen, Z. Zhang, W. Qiao, D. Long and L. Ling, *ACS Catal.*, 2013, **3**, 862.
 - 36 L. Hao, B. Luo, X. Li, M. Jin, Y. Fang, Z. Tang, Y. Jia, M. Liang, A. Thomas, J. Yang and L. Zhi, *Energy Environ. Sci.*, 2012, **5**, 9747.
 - 37 Z. Xiong and X. S. Zhao, *J. Am. Chem. Soc.*, 2012, **134**, 5754.
 - 38 J.-e. Park, E. D. Grayfer, Y. Jung, K. Kim, K.-K. Wang, Y.-R. Kim, D. Yoon, H. Cheong, H.-E. Chung, S.-J. Choi, J.-H. Choy and S.-J. Kim, *J. Mater. Chem. B*, 2013, **1**, 1229.
 - 39 S. Feng, W. Li, Q. Shi, Y. Li, J. Chen, Y. Ling, A. M. Asiri and D. Zhao, *Chem. Commun.*, 2014, **50**, 329.
 - 40 J. Wang, I. Senkowska, M. Oschatz, M. R. Lohe, L. Borchardt, A. Heerwig, Q. Liu and S. Kaskel, *J. Mater. Chem. A*, 2013, **1**, 10951.
 - 41 D. Wei, Y. Liu, Y. Wang, H. Zhang, L. Huang and G. Yu, *Nano Lett.*, 2009, **9**, 1752.
 - 42 D. Long, W. Li, L. Ling, J. Miyawaki, I. Mochida and S.-H. Yoon, *Langmuir*, 2010, **26**, 16096.
 - 43 S. Wang, X. Zhao, T. Cochell and A. Manthiram, *J. Phys. Chem. Lett.*, 2012, **3**, 2164.
 - 44 J. Tang, T. Wang, X. Pan, X. Sun, X. Fan, Y. Guo, H. Xue and J. He, *J. Phys. Chem. C*, 2013, **117**, 16896.
 - 45 Y. Zhao, R. Nakamura, K. Kamiya, S. Nakanishi and K. Hashimoto, *Nat. Commun.*, 2013, **4**, 2309.
 - 46 D. H. Shin, J. Lee, J. Jun and J. Jang, *J. Mater. Chem. A*, 2013, **2**, 3364.
 - 47 Y. D. Xia and R. Mokaya, *Adv. Mater.*, 2004, **16**, 1553.
 - 48 A. H. Lu, A. Kiefer, W. Schmidt and F. Schuth, *Chem. Mater.*, 2004, **16**, 100.
 - 49 L. Hou, L. Lian, D. Li, G. Pang, J. Li, X. Zhang, S. Xiong and C. Yuan, *Carbon*, 2013, **64**, 141.
 - 50 B. Xu, S. Hou, G. Cao, F. Wu and Y. Yang, *J. Mater. Chem.*, 2012, **22**, 19088.
 - 51 L. Zhao, N. Baccile, S. Gross, Y. Zhang, W. Wei, Y. Sun, M. Antonietti and M.-M. Titirici, *Carbon*, 2010, **48**, 3778.
 - 52 Z. Lu, W. Zhu, X. Lei, G. R. Williams, D. O'Hare, Z. Chang, X. Sun and X. Duan, *Nanoscale*, 2012, **4**, 3640.
 - 53 J. Xu, S. Gai, F. He, N. Niu, P. Gao, Y. Chen and P. Yang, *J. Mater. Chem. A*, 2014, **2**, 1022.
 - 54 M. Shao, F. Ning, Y. Zhao, J. Zhao, M. Wei, D. G. Evans and X. Duan, *Chem. Mater.*, 2012, **24**, 1192.
 - 55 L. Wang, D. Wang, X. Y. Dong, Z. J. Zhang, X. F. Pei, X. J. Chen, B. Chen and J. Jin, *Chem. Commun.*, 2011, **47**, 3556.
 - 56 Z. Gao, J. Wang, Z. Li, W. Yang, B. Wang, M. Hou, Y. He, Q. Liu, T. Mann, P. Yang, M. Zhang and L. Liu, *Chem. Mater.*, 2011, **23**, 3509.
 - 57 W. Stöber, A. Fink and E. Bohn, *J. colloid interf. Sci.*, 1968, **26**, 62.
 - 58 S. Tan, P. Yang, N. Niu, S. Gai, J. Wang, X. Jing and J. Lin, *J. Alloys and Compd.*, 2010, **490**, 684.
 - 59 B. Guan, X. Wang, Y. Xiao, Y. Liu and Q. Huo, *Nanoscale*, 2013, **5**, 2469.
 - 60 M. Shao, F. Ning, J. Zhao, M. Wei, D. G. Evans and X. Duan, *J. Am. Chem. Soc.*, 2012, **134**, 1071.
 - 61 Y. Zhao, S. He, M. Wei, D. G. Evans and X. Duan, *Chem. Commun.*, 2010, **46**, 3031.
 - 62 P. Lv, H. Zhao, J. Wang, X. Liu, T. Zhang and Q. Xia, *J. Power Source*, 2013, **237**, 291.
 - 63 J. Yang, C. Yu, X. Fan, Z. Ling, J. Qiu and Y. Gogotsi, *J. Mater. Chem. A*, 2013, **1**, 1963.
 - 64 M. Seredych, D. Hulicova-Jurcakova, G. Q. Lu and T. J. Bandosz, *Carbon*, 2008, **46**, 1475.
 - 65 D. Hulicova-Jurcakova, M. Kodama, S. Shiraiishi, H. Hatori, Z. H. Zhu and G. Q. Lu, *Adv. Funct. Mater.*, 2009, **19**, 1800.
 - 66 G. Q. Zhang, H. B. Wu, H. E. Hoster, M. B. Chan-Park and X. W. Lou, *Energy Environ. Sci.*, 2012, **5**, 9453.
 - 67 H. Guo and Q. Gao, *J. power Source*, 2009, **186**, 551.
 - 68 V. V. Strelko, V. S. Kuts and P. A. Thrower, *Carbon*, 2000, **38**, 1499.

-
- 69 D.-W. Wang, F. Li, L.-C. Yin, X. Lu, Z.-G. Chen, I. R. Gentle, G. Q. Lu and H.-M. Cheng, *Chem. Eur. J.*, 2012, **18**, 5345.
- 70 G. Wang, J. Huang, S. Chen, Y. Gao and D. Cao, *J. Power Source*, 2011, **196**, 5756.